Electronic Supplementary Information (ESI) for Nanoscale.
This journal is © The Royal Society of Chemistry

Supporting Information

Visualization of polar nanoregions in lead-free relaxors via piezoresponse force microscopy in torsional dual AC resonance tracking mode

Na Liu,[a,b] Robert Dittmer,[c] Robert W. Stark*[a,b] and Christian Dietz*[a,b]

[a]*Institute of Materials Science, Physics of Surfaces, Alarich-Weiss-Str. 2, 64287 Darmstadt, Germany*

[b]*Center of Smart Interfaces, Technische Universität Darmstadt, Alarich-Weiss-Str. 10, 64287 Darmstadt, Germany*

[c]*Institute of Materials Science, Nichtmetallische-Anorganische Werkstoffe, Technische Universität Darmstadt, Alarich-Weiss-Str. 2, 64287 Darmstadt, Germany*

Resonance tune in torsional dual AC resonance tracking mode.

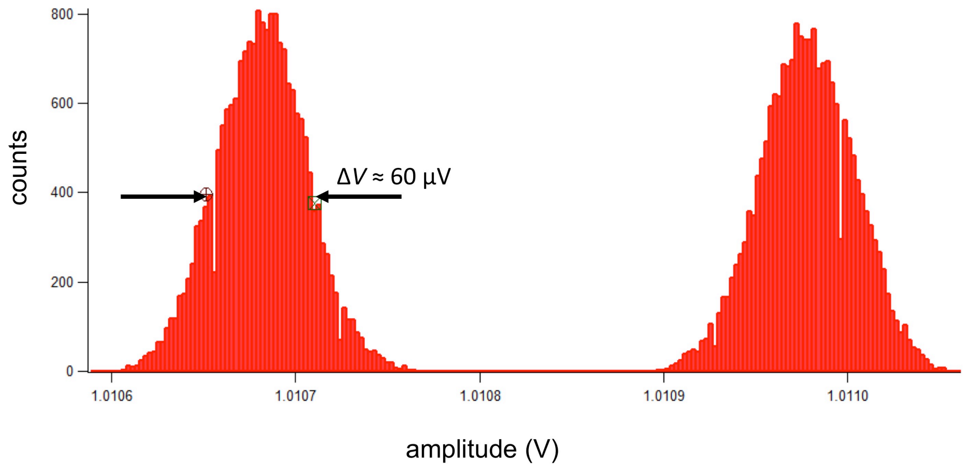

Fig. S1 Estimation of the amplitude resolution. To estimate the amplitude resolution the drive amplitude was stepped between two values. The output of the lock-in amplifier (measured amplitude) is shown as a histogram. The histogram shows a bimodal distribution around both driving amplitude values. The full width at half maximum of the peaks (~ 60 µV) is mainly determined by noise, digitalization and the transient response of the circuitry. It thus provides a rough estimate for the minimum detectable amplitude difference (the bandwidth filter was set to 5 kHz).

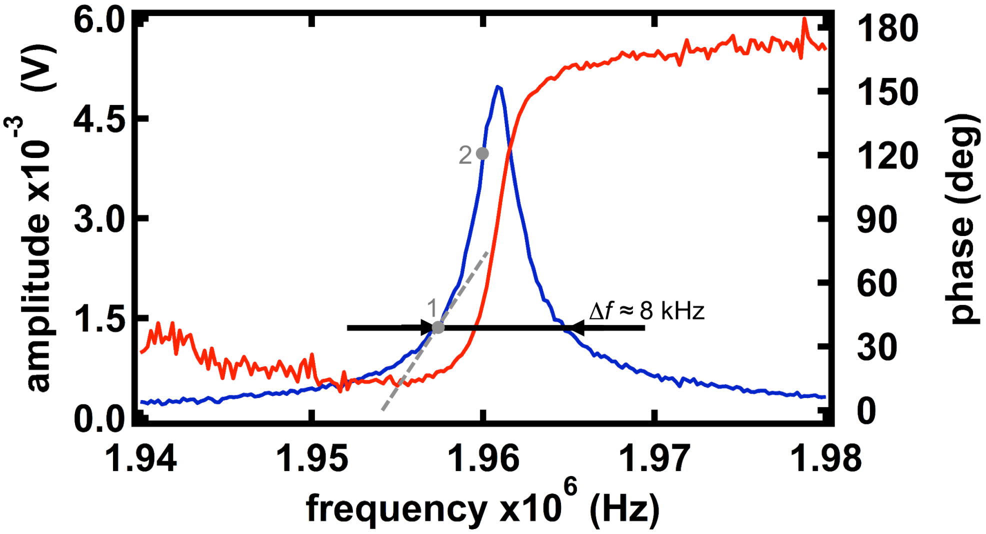

Fig. S2 Amplitude (blue, left axis) and phase (red, right axis) versus excitation frequency of the torsional vibration of an ASYELEC-02 (Asylum Research, Santa Barbara, USA) cantilever on a 3BMT sample surface applying an AC voltage 3 V to the tip. The frequency range for the frequency feedback loop is indicated by the arrows. Point 1 marks the detection point for the amplitude at f_1. The inverse slope ($S_1^{-1} = \mathrm{d}f_1/\mathrm{d}A_1 \approx 2890$ Hz/mV) is marked by the gray dashed line determining the minimum detectable frequency shift. The maximum slope (minimum inverse slope) of the resonance curve can be found at point 2 ($S_2^{-1} = \mathrm{d}f_2/\mathrm{d}A_2 \approx 465$ Hz/mV)

Macroscopic characteristics of $0.81Bi_{1/2}Na_{1/2}TiO_3$-$0.19Bi_{1/2}K_{1/2}TiO_3$ (0BMT) and $0.97(0.81Bi_{1/2}Na_{1/2}TiO_3$-$0.19Bi_{1/2}K_{1/2}TiO_3)$-$0.03BiMg_{1/2}Ti_{1/2}O_3$ (3BMT).

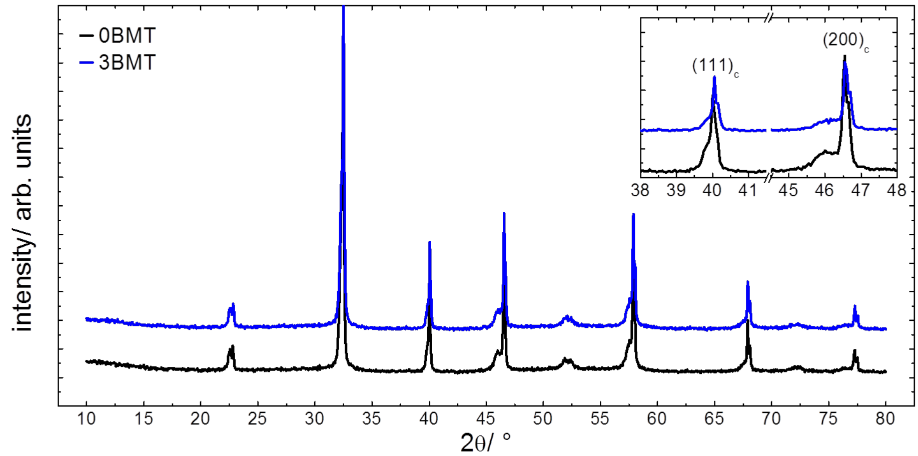

Fig. S3 X-ray diffraction pattern for 0BMT and 3BMT poled at 6 kV/mm. The inset shows the $\{111\}_c$ and the $\{200\}_c$ reflection of both materials.

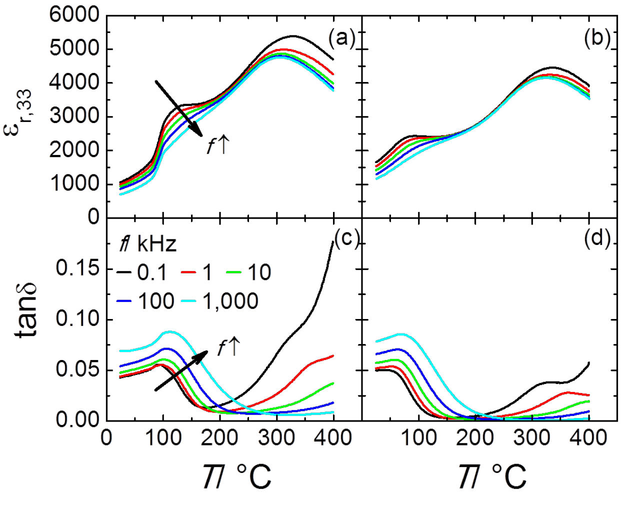

Fig. S4 Relative dielectric permittivity (top row) and loss tangent *tan δ* (bottom row) at various frequencies for 0BMT (a and c) and 3BMT (b and d) in the poled state from room temperature up to 400 °C.

Increased reliability of the image and reduced topographical crosstalk of dual AC resonance tracking in the cantilever's torsional vibration mode.

The Fig. S5 shows the phase response of the same area measured by SF- (a) and TDART-(b) PFM, as well as the respective cross-sectional profiles (c). Both images feature two dominant phase values that can be attributed to the two possible domain orientations in the particular direction of the observation. A bright dot (encircled by the blue circle) directly below the central domain is visible in the SF-PFM image. Highlighted by the blue ellipse and the arrows in the cross-section, the phase profile measured by SF-PFM clearly deviates from the profile obtained by TDART with a bump/hollow combination rather than a flat area at the same position. The associated topography image (see inset of Fig. S5(c)) exhibits a hole approximately 500 pm in depth at this exact position. For clarity, we added the topographical profile into the cross-section, which indicates the correlation between the height and phase. In the case of the SF-PFM technique, this artifact was caused by topographical crosstalk induced by the feedback loop keeping the mean deflection signal constant during scanning. At the falling edge, the deflection of the cantilever changes to lower values, forcing the *z*-piezo to move the tip towards the sample surface to trace the topography. A sloped topography, however, can only be tracked with residual error. As a consequence, the contact resonance shifts to lower frequencies and hence the phase shifts to larger values compared to the contact resonance corresponding to the given deflection set point (note that the phase data shown in Fig S5 corresponds to the retrace curve, *i.e.*, the scan direction was from right to left). At the rising edge, the topography error has the opposite sign; thus, the contact resonant frequency shifts to higher values and smaller phase shifts. These variations lead to a wave-like shape of the phase shift profile in SF-PFM as shown in Fig. S5(a). In TDART mode, however, this artifact is corrected by the additional feedback loop tracking the instantaneous contact resonance. In addition, the slope derived from the phase profile obtained by TDART (red) is higher than that measured by the SF technique at the right domain wall between the central and outer domains, corroborating the higher lateral resolution for the TDART mode previously confirmed by the amplitude signal. The fit of the experimental phase data resulted in a domain wall width of (38 ± 3) nm for the TDART mode and (42 ± 2) nm for the SF technique (see main article for details).

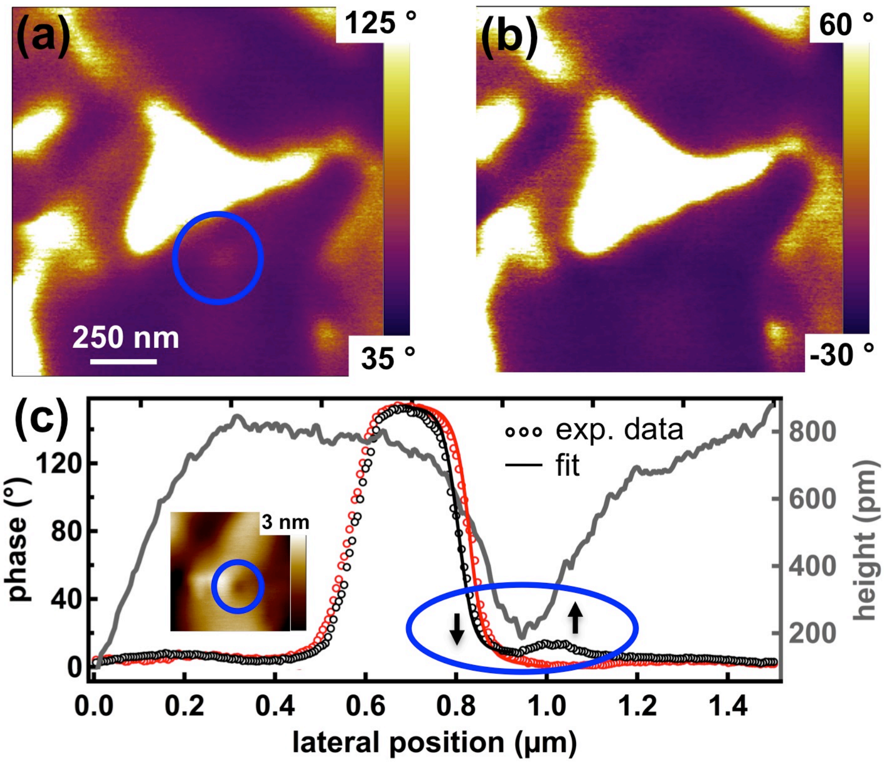

Fig. S5 Comparison between the phase signals of the 0BMT sample surface measured by (a) SF- and (b) TDART-PFM modes. (c) Cross-sectional profiles of the SF-PFM (black dots) and TDART-PFM (red dots) phase signals. The gray line corresponds to the respective topographical profile. The inset in (c) shows the topographical image, in which the encircled area is the position of the hollow in the profile. Upward and downward arrows show the falling and rising edges of the hole, which had to be compensated by the feedback loop, leading to imaging artifacts. The black and red solid lines correspond to the fit data for the phase values at the right domain wall (phase data was shifted for the fit).

Resolution of nanoscale features

In principle, noise and feedback lagging or ringing might cause very tiny features in the amplitude and phase images that can be misinterpreted as PNRs. To corroborate the detectability of PNRs by TDART, we focused on nanoscale features prevailing in the amplitude images. These features were repeatedly scanned at scan angles parallel and perpendicular to the cantilever axis. Figure S7 shows the topography (top row), amplitude (middle row) and phase images (bottom row) of a 3BMT sample measured by SF-PFM (left two columns) and TDART-PFM (right two columns). The left column for each mode was obtained by scanning at an angle of $\alpha_{scan} = 0°$, *i.e.* with the fast scan axis in the same direction as the long axis of the cantilever, whereas the right column was scanned perpendicular to the cantilever axis. The features indicated by the arrows appear in both images irrespective of the scan direction. This clearly indicates that the nanoscale features are not caused by the noise or feedback induced artifacts. Furthermore, these nanoscale features are hardly visible in the amplitude image obtained by the SF-PFM mode. Notably, the orientation of some features apparent in the phase images measured by SF-PFM strongly depends on the scan direction as indicated by the encircled area (left two images, bottom row).

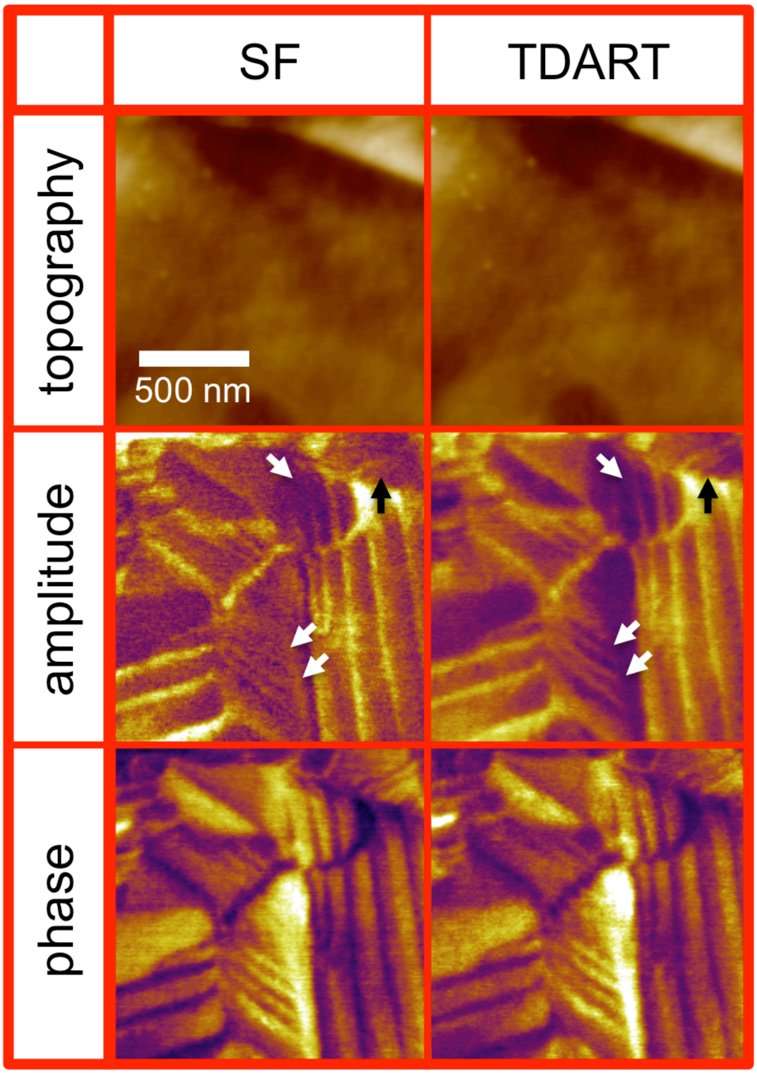

Fig. S6. Comparison between the SF-PFM (left column) and the TDART techniques (right column). Shown are the topography (top row), amplitude (middle row) and phase (bottom row) images obtained on piezoelectric standard material PIC 151 (lead-zirconate-titanate, PZT). The TDART amplitude image clearly reveals a riffled structure that could not be resolved by SF-PFM (see locations indicated by the arrows). The corresponding phase images exhibit the same lateral distribution of ferroelectric in-plane domains.

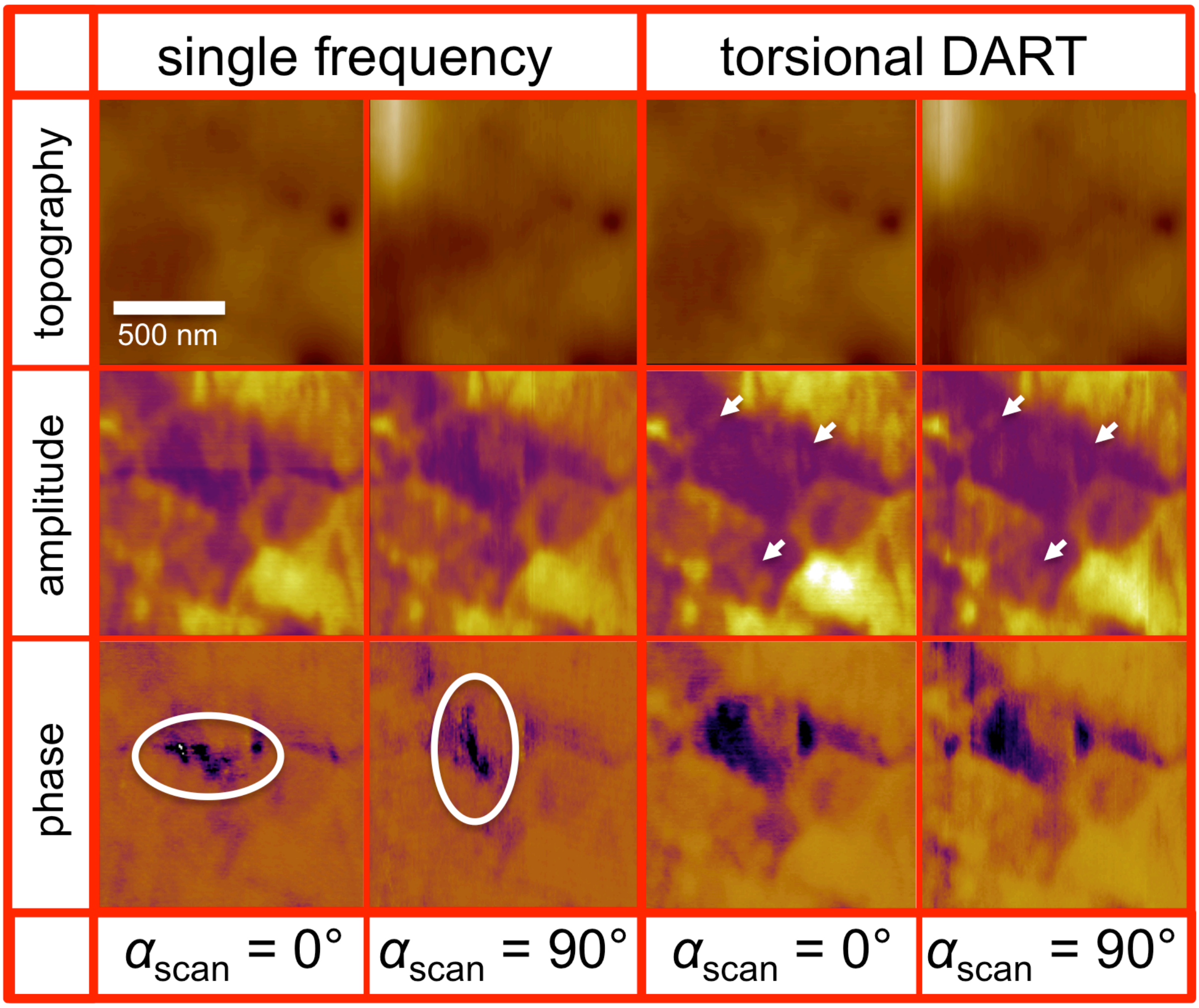

Fig. S7 Comparison between the SF-PFM mode (left two columns) and the TDART technique (right two colums). Topography (top row), amplitude (middle) and phase (bottom) images of a 3BMT sample. The images were measured in different scan directions as noted at the bottom. Arrows indicate similar features that are independent of the scan direction with respect to the sample, whereas the encircled areas highlight a region showing a domain orientation that indeed depends on the scan direction. Color bars: topography 0–8 nm, amplitude arbitrary, phase -19–58 °, -16–54 °, 53–233 °, 48–228 ° (from left to right).